J Mater Sci (2006) 41:6313–6321
DOI 10.1007/s10853-006-0500-2

Analysis of cracking of lithium tantalate ($LiTaO_3$) single crystals due to thermal stress

N. Miyazaki · N. Koizumi

Received: 14 January 2004 / Accepted: 30 August 2005 / Published online: 12 August 2006

Abstract Quantitative estimation of failure of a $LiTaO_3$ single crystal due to thermal stress was investigated. Cylindrical test slabs were heated in a silicone oil bath, then subjected to large thermal stress by pouring silicone oil with room temperature. Cracking occurred during cooling. A transient heat conduction analysis was performed to obtain a temperature distribution in a test slab at the time of cracking, using the surface temperatures measured in the test. Then thermal stress was calculated using a temperature profile of the test slab obtained from the heat conduction analysis. It is found from the results of thermal stress analyses and the observation of the cracking in the test slabs that the cracking induced by thermal stress occurs mainly in the cleavage planes due to the stress component normal to the plane. As for a size effect of failure stress, large-sized cylindrical test slabs show lower failure stress than small-sized ones. Four-point bending tests were also performed to examine the relationship between the critical stress for cracking induced by thermal stress and the four-point bending strength. A useful relation was derived for predicting the critical stress for cracking induced by thermal stress from the four-point bending strength.

N. Miyazaki (✉)
Department of Mechanical Engineering and Science,
Kyoto University, Yoshida-Honmachi, Sakyo-ku,
Kyoto 606-8501, Japan
e-mail: miyazaki@mech.kyoto-u.ac.jp

N. Koizumi
Department of Material Process Engineering,
Kyushu University, 6-10-1 Hakozaki, Higashi-ku,
Fukuoka 812-8581, Japan

Introduction

Trigonal oxide single crystals such as lithium niobate ($LiNbO_3$, abbreviated as LN) and lithium tantalate ($LiTaO_3$, abbreviated as LT) are used not only as materials for surface acoustic wave (SAW) devices but also as materials for photonic devices. Their bulk single crystals are usually manufactured by the Czochralski (CZ) growth technique. Cracking of such bulk single crystals sometimes occurs during the CZ growth process, especially during cooling [1–3]. Such cracking can be caused by thermal stress during crystal growth process. Thermal stress analyses of LN bulk single crystals [2, 4–6] have been performed from the viewpoint of the cracking and quality of single crystals. Among them, Galazka [4] obtained analytically a time-dependent stress field in an LN single crystal immediately after its extraction from melt, and he found that the magnitude of the stress caused by the thermal shock depends mainly on the crystal diameter, its thermal conductivity and the axial temperature gradient in the growth system. Miyazaki et al. [5] performed thermal stress analyses of LN bulk single crystals during the CZ growth process to study the effect of the growth direction of a single crystal on the thermal stress. In these analyses, three-dimensional finite element method was employed to take account of crystal anisotropy in the elastic constants and thermal expansion coefficients. Based on the results, they made a discussion on the relationship between the growth direction and the cracking and quality of a single crystal. After that, Kobayashi et al. [6] combined the method of thermal stress analysis proposed by Miyazaki et al. [5] with the global heat transfer analysis in a CZ furnace. They found that the thermal stress has

a minimum near a critical Reynolds number, at which the melt/crystal interface inversion occurs. Only quantitative discussions on the relationship between the thermal stress and the cracking and quality of single crystals are made in the papers mentioned above. For quantitative discussions on the cracking, a critical value for the cracking must be obtained from experiments. We performed cracking experiments under thermal loading conditions, using LN bulk single crystals [7] and gadolinium orthosilicate (Gd_2SiO_5, abbreviated as GSO) bulk single crystals [8]. In these experiments, we could not discuss a size effect on the cracking induced by thermal stress, because we used test slabs with the same size.

In the present study, we prepared three kinds of LT test slabs with different sizes, and carried out thermal stress tests to induce cracking. Then thermal stress analyses considering crystal anisotropy were performed to obtain a critical stress for the cracking, using temperature data obtained from the thermal stress tests. Based on the results, we discussed the size effect on the cracking due to thermal stress from the viewpoint of the Weibull's weakest link model. Four-point bending tests were also carried out to examine the relationship between the critical stress for the cracking induced by thermal stress and the four-point bending strength.

Experimental procedure

Thermal stress tests

Figure 1 shows the apparatus for the thermal stress tests. Cylindrical test slabs were cut from an LT bulk single crystal pulled along the axis inclined by 36 degrees from the crystallographic *Y*-axis to *Z*-axis. The cleavage planes in the test slab are shown in Fig. 2. All surfaces of the test slabs were polished like mirror.

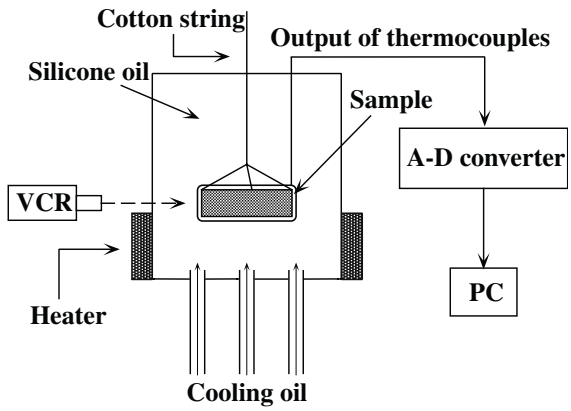

Fig. 1 Apparatus for thermal stress test

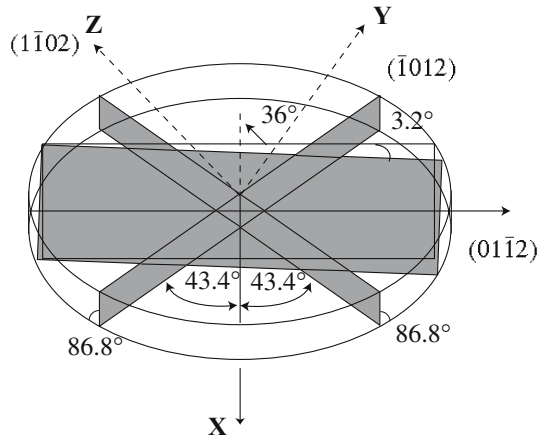

Fig. 2 Cleavage planes of LT single crystal

Three kinds of the test slabs with different sizes were used, that is, Case 1 (small-sized slabs): 50 mm in diameter and 10 mm in height, Case 2 (medium-sized slabs): 75 mm in diameter and 10 mm in height, and Case 3 (large-sized slabs): 75 mm in diameter and 20 mm in height.

A test slab was heated to about 470 K in a bath filled with silicone oil, then thermal stress was applied to it by pouring silicone oil with a room temperature into heated oil bath, and cracking occurred during cooling due to thermal stress. The surface temperatures were measured using thermocouples attached on the surfaces of the test slab and all the measured temperatures were recorded in a personal computer (PC) via an analog-to-digital converter. Figure 3 shows the locations of temperature measurement. The time when the cracking occurred was identified by a video cassette recorder (VCR).

Four-point bending tests

Four-point bending tests were carried out at a temperature of 470 K and at a displacement rate of 0.2 mm/min. Figure 4 shows a test jig and a cleavage plane in a test specimen. The test specimens were 50 mm in length, 10 mm in width and 1 mm in thickness. All

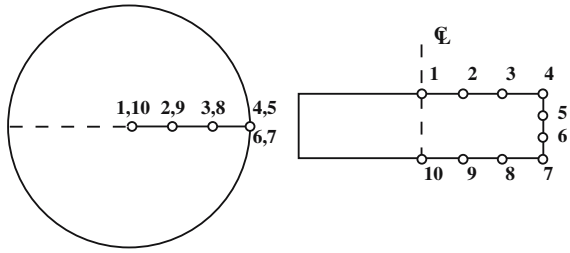

Fig. 3 Locations of temperature measurement

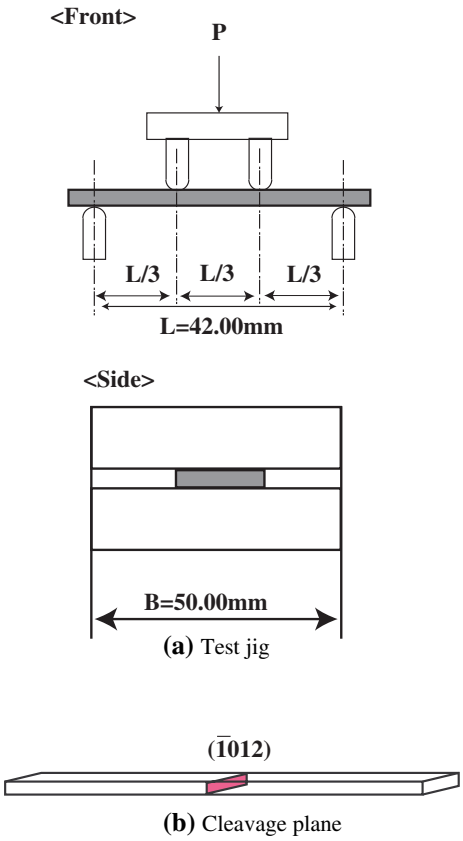

Fig. 4 Four point bending test for LT single crystal. (**a**) Test jig (**b**) Cleavage plane

surfaces of the test specimens were polished like mirror. A cleavage plane is nearly normal (86.8°) to upper and lower surfaces and exactly normal to the longitudinal direction of the specimen, as shown in Fig. 4b.

Analytical procedure

A flowchart for evaluation of the thermal stress test results is shown in Fig. 5. A transient heat conduction analysis is performed to obtain the temperature distribution in an LT test specimen, using the surface temperatures measured in the thermal stress test. A thermal stress analysis is then performed, based on the results of the heat conduction analysis. Finally the stress is converted into several stresses for failure evaluation.

Heat conduction analysis

Finite element heat conduction analyses for an axisymmetric body were performed to obtain temperature distributions in LT test slabs at the time of cracking. These analyses used the eight-noded isoparameteric

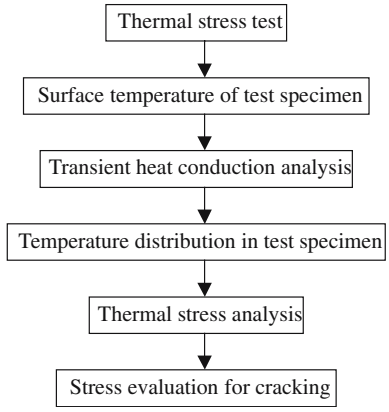

Fig. 5 Flowchart for evaluation of thermal stress test results

elements, that is, 810 elements and 2557 nodes for Case 1 and 1224 elements and 3845 nodes for Case 2 and Case 3. The surface temperatures were prescribed as a boundary condition, using the temperature data on the crystal surface measured in the thermal stress tests. The density ρ, specific heat C_p and thermal conductivity λ of an LT single crystal are required for the heat conduction analysis. They were determined by the literatures survey, that is, ρ from Smith and Welsh [9], and C_p and λ from Lin et al. [10].

$$\rho = 7.45 \times 10^5\,\mathrm{kg/m^3},$$
$$C_p = 443\,\mathrm{J/(kg \cdot K)},$$
$$\lambda = 1.41\,\mathrm{W/(m \cdot K)}$$

Thermal stress analysis

Details of thermal stress analysis are already given in [5, 7, 11]. In the present paper, we will explain it briefly. An LT single crystal belongs to a trigonal class 3 m single crystal. When a right-handed Cartesian coordinate system X_1–X_2–X_3 is taken in such a way that the X_1-axis and the X_3-axis coincide with the crystallographic X-axis and Z-axis, respectively, as shown in Fig. 6a, the elastic constant matrix $[C_{ij}]$ is written as follows [12]:

$$[C_{ij}] = \begin{bmatrix} C_{11} & C_{12} & C_{13} & C_{14} & 0 & 0 \\ & C_{11} & C_{13} & -C_{14} & 0 & 0 \\ & & C_{33} & 0 & 0 & 0 \\ & & & C_{44} & 0 & 0 \\ & \mathrm{sym} & & & C_{44} & C_{14} \\ & & & & & C_{66} \end{bmatrix}$$

$$C_{66} = \frac{1}{2}(C_{11} - C_{12}) \quad (1)$$

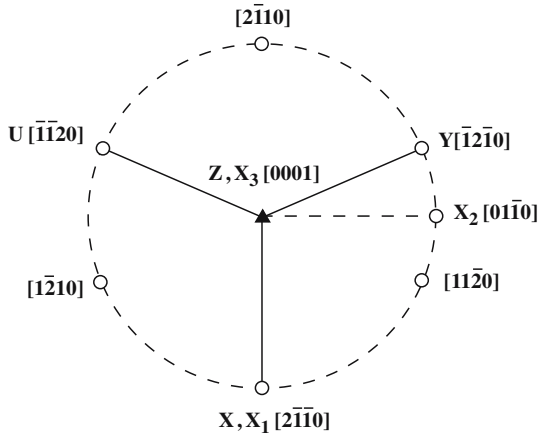

(a) Stereographic projection

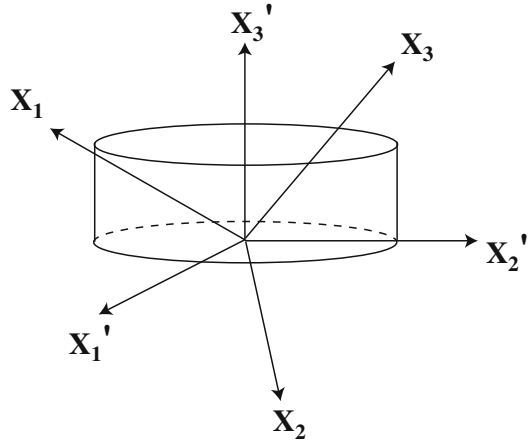

(b) Coordinate systems for thermal stress analysis

Fig. 6 Relation between coordinate systems. (**a**) Stereographic projection (**b**) Coordinate systems for thermal stress analysis

Let us consider a right-handed Cartesian coordinate system X'_1–X'_2–X'_3 shown in Fig. 6b, where the X'_1-axis is in the X_1–X_2 plane and normal to the X'_3-axis. By the standard tensor transformation, the elastic constant tensors C'_{ijkl} associated with the X'_1–X'_2–X'_3 system are related to C_{ijkl} of the X_1–X_2–X_3 system as follows:

$$C'_{ijkl} = a_{im}a_{jn}a_{ko}a_{lp}C_{mnop} \tag{2}$$

A trigonal class 3 m single crystal has anisotropy in the thermal expansion coefficients as well as in the elastic constants. It has different values of the thermal expansion coefficient in the Z-axis (α_{33}) and in the plane normal to the Z-axis (α_{11}). Using the standard tensor transformation, the thermal expansion coefficient tensors α'_{ij} in the X'_1–X'_2–X'_3 system are given as follows:

$$\alpha'_{ij} = a_{ik}a_{jl}a_{kl} \tag{3}$$

We can perform a thermal stress analysis of a trigonal class 3 m single crystal in the coordinate system X'_1–X'_2–X'_3, using C'_{ijkl} and α'_{ij}.

The finite element model for a three-dimensional thermal stress analysis of an LT test slab are shown in Fig. 7, where one quarter region is cut in order to show the internal part clearly. Thermal stress analyses used the 20-noded isoparameteric elements, that is, 1920 elements and 9293 nodes for Case 1, 3080 elements and 14575 nodes for Case 2, and 3200 elements and 14805 nodes for Case 3. Table 1 shows the elastic constants C_{ij} [13], thermal expansion coefficients α_i [9] and melting point T_f [13] of an LT single crystal.

Stress evaluation for cracking

The thermal stress at the time of cracking obtained from the analysis was converted into the following stresses to discuss the cracking induced by thermal stress; (a) Mises equivalent stress $\sqrt{3J'_2}$, where J_2' is the second invariant of deviatoric stresses, (b) the maximum principal stress σ_1, (3) the maximum normal stress σ_n acting on the cleavage planes, and (4) the maximum shear stress σ_s acting on the cleavage planes.

Results and discussion

Thermal stress tests

We carried out multiple runs of the thermal stress tests for the respective test slabs, Case 1, Case 2 and Case 3. Figure 8 shows an example of the time variations of surface temperatures measured by thermocouples that are attached to the locations 1, 6 and 8 shown in Fig. 3.

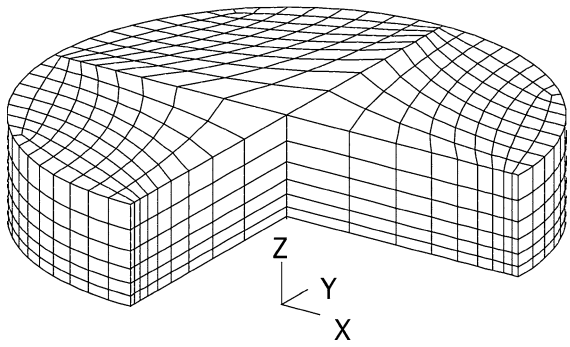

Fig. 7 Finite element mesh for three-dimensional thermal stress analysis

Table 1 Elastic constants, thermal expansion coefficients and melting point of LT single crystal

Constant	Value	Unit
C_{11}	230×10^3	[MPa]
C_{12}	42×10^3	[MPa]
C_{13}	79×10^3	[MPa]
C_{14}	-11×10^3	[MPa]
C_{33}	276×10^3	[MPa]
C_{44}	96×10^3	[MPa]
α_1	16.1×10^{-6}	[K^{-1}]
α_3	4.1×10^{-6}	[K^{-1}]
T_f	1923	[K]

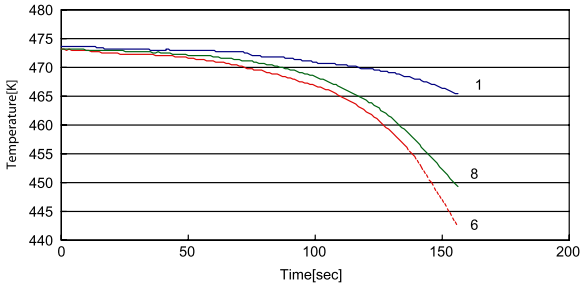

Fig. 8 Time variations of surface temperatures measured by thermocouples: Case 1, No. 4

The origin of time is defined at the time when silicone oil of a room temperature begins to flow into hot silicone oil. In this case, the cracking of a test slab occurs at the time of 156 s. Using these measured temperatures, transient heat conduction analyses were performed to obtain the temperature distribution at the time of cracking. An example of the calculated result is shown in Fig. 9. The lower rim of a test slab is well cooled and a large temperature gradient is found there. Figure 10 shows an example of the distribution of the maximum normal stress σ_n acting on the cleavage planes at the time of cracking. Corresponding to the temperature distribution, large stresses are found near the lower rim of a test slab.

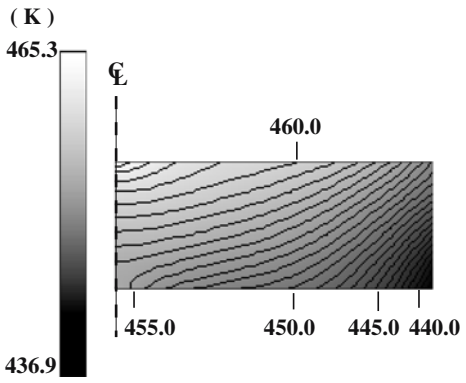

Fig. 9 Temperature distribution obtained from heat conduction analysis (ΔT = 1.0 K): Case 1, No. 4

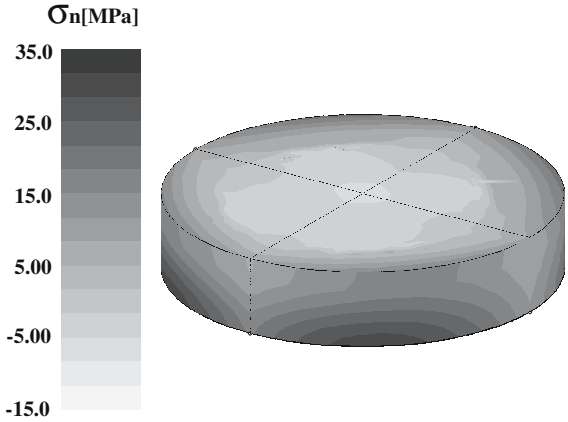

Fig. 10 Distribution of σ_n at the time of cracking obtained from thermal stress analysis: Case 1, No. 4

Table 2 summarizes the maximum values of stress at the cracking for the respective test slabs. The cracking due to thermal stress is shown in Fig. 11 for each case. In Case 1, it was examined by X-ray diffraction whether or not crack a surface coincides with a cleavage plane. In Case 2 and Case 3, a pair of cleavage planes was marked on the surface on a test slab. In these cases, it was examined by comparing the cracking with this marking whether or not a crack surface coincides with a cleavage plane. That is, if the cracking occurs in parallel with this marking and nearly normal to upper and lower surface of a slab, a crack surface is confirmed to coincide with a cleavage plane. As shown in Fig. 11a, b, the cracking starts to occur at the rim of a

Table 2 Maximum values of stress at cracking

No.	σ_1 [MPa]	$\sqrt{3J_2'}$ [MPa]	σ_n [MPa]	σ_s [MPa]
(a) Case 1: Small-sized specimens				
1	65.3	65.4	58.3	32.7
2	47.6	47.6	44.8	23.8
3	54.1	54.2	49.9	27.1
4	33.2	33.2	30.7	16.6
5	39.2	35.9	35.9	19.6
6	64.6	64.8	58.1	32.0
(b) Case 2: Medium-sized specimens				
1	44.4	43.9	43.0	22.2
2	35.3	34.7	32.8	17.7
3	48.7	48.8	44.2	24.2
4	31.1	31.1	30.2	15.4
5	28.3	28.4	25.4	14.1
6	50.8	52.9	45.1	28.2
7	61.4	61.4	57.9	30.7
(c) Case 3: Large-sized specimens				
1	38.8	38.9	35.8	19.4
2	41.7	40.7	38.1	20.8
3	71.1	70.9	64.8	35.6
4	33.4	32.0	31.5	16.7
5	27.7	27.9	26.3	13.9
6	36.4	35.6	32.7	18.2

(a) Case 1, No. 4 : small-sized slab

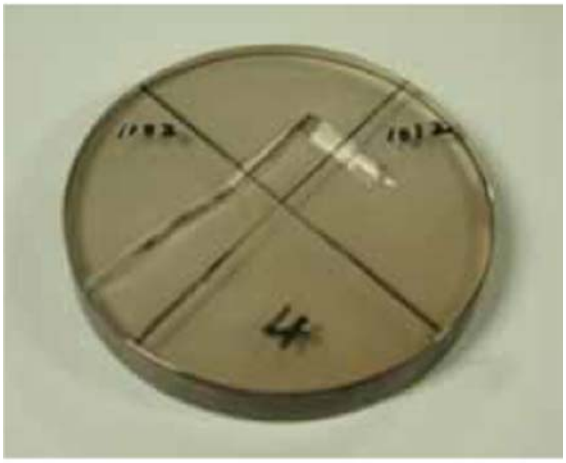

(b) Case 2, No. 3 : medium-sized slab

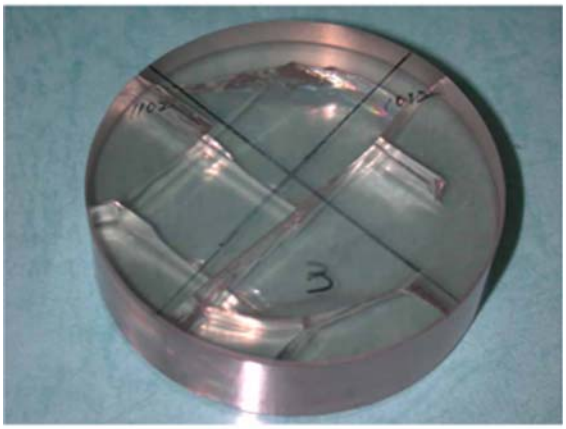

(c) Case 3, No. 3 : large-sized slab

Fig. 11 Cracking due to thermal stress. (**a**) Case 1, No. 4: small-sized slab. (**b**) Case 2, No. 3: medium-sized slab. (**c**) Case 3, No. 3: large-sized slab

specimen and propagates along cleavage planes in Case 1 and Case 2. In Case 3, large-sized slabs, the cracking is a little bit complicated. As shown in Fig. 11c, several cracks can be seen besides the cracks coincident with the cleavage planes. Although multiple cracks are observed in some test slabs, the cracking occurs mainly in the cleavage planes. From the viewpoint of material strength of brittle materials or fracture mechanics, the tensile stress normal to a crack surface induces the cracking. As described above, we can observe that the cracking occurred mainly at the cleavage plane. It is therefore concluded that, among various stresses shown in Table 2, the stress normal to the cleavage plane σ_n dominates the cracking due to thermal stress.

Four-point bending tests

Four-point bending tests were performed for eight test specimens. Figure 12 shows the failure observed in the tests. Table 3 summarizes the four-point bending strength σ_b. As shown in Fig. 4b, a cleavage plane is located in the cross section nearly normal (86.8°) to the upper and lower surfaces and normal to the longitudinal axis. It is therefore expected that failure occurs at this cleavage surface. The failure observed in the test was not normal to the longitudinal axis, as shown in Fig. 12. This fact means that the failure does not occur at the cleavage plane. This may be because brittle failure preceded cleavage failure owing to thin thickness.

Size effect on cracking

Generally speaking, failure strength of a brittle material is dominated by small defects in the material, and its failure strength deviates greatly due to the deviation of the defect size. The deviation of the maximum value of σ_n at the time of cracking shown in Table 2 may be due to this reason, so it is appropriate to deal with the failure data statistically. Statistical analyses were

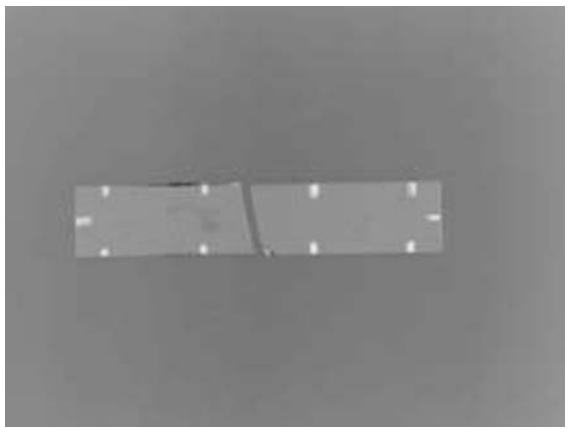

Fig. 12 Failure observed in four-point bending tests: No. 6 specimen

Table 3 Four-point bending strength

No.	Bending strength σ_b [MPa]
1	118.7
2	176.2
3	127.2
4	94.2
5	98.3
6	110.4
7	106.4
8	143.7

performed by the Weibull plots of the failure data obtained from the thermal stress tests and the four-point bending tests [14, 15]. These Weibull plots are shown in Fig. 13, where cumulative failure probability

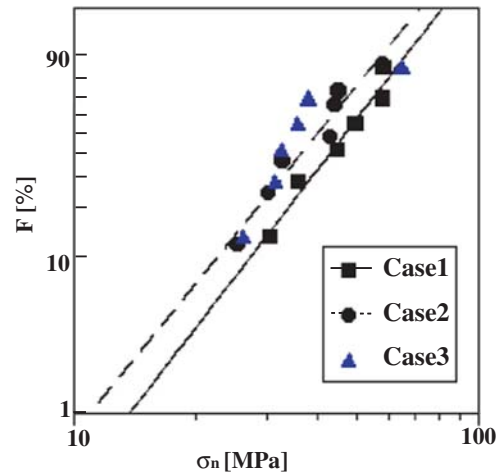

(a) Thermal stress tests

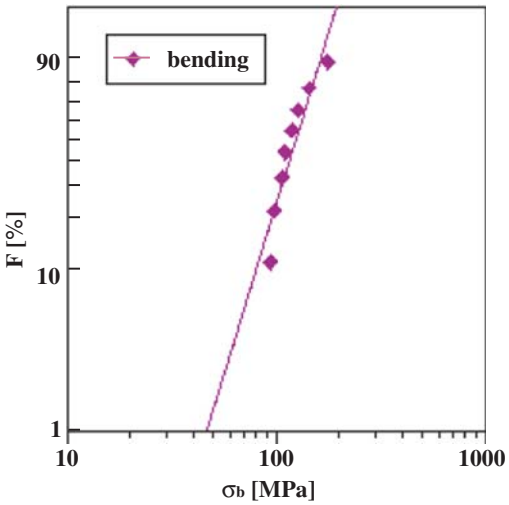

(b) Four-point bending tests

Fig. 13 Weibull plots for thermal stress tests and four-point bending tests. (**a**) Thermal stress tests. (**b**) Four-point bending tests

F is related to the stress σ_n shown in Table 2 for the thermal stress tests and the stress σ_b shown in Table 3 for the four-point bending tests. The failure data show good linearity and obey the Weibull distribution except for Case 3 of the thermal stress tests. In Case 3, there exist other brittle failures besides the failures generated in the cleavage planes. This may be the reason why Case 3 does not obey the Weibull distribution.

According to the Webull distribution's weakest link model, the strength of a brittle material is dominated by the maximum size of the defects being subjected to tensile stress, and the probability of large-sized defects containing in a material increases as the size of a material increases. Consequently, a larger specimen has a lower failure stress. This may be the reason why the failure data of Case 2 and Case 3 scatter at lower stress level than those of Case 1, as shown in Fig. 13a. As for Case 1 and Case 2, they have almost the same slope of the Weibull plots, that is, 3.48 for Case 1 and 3.30 for Case 2, which indicates that the Weibull distribution of Case 2 can be estimated from that of Case 1 by correcting a size effect. For this correction, we used a return period T defined by $T = S_2/S_1$, where S_1 and S_2 are effective areas for Case 1 and Case 2, respectively. In the thermal stress tests, the origin of cracking is the rim surface of a cylindrical slab, so we chose the area of the rim surface as an effective area. The broken line in Fig. 14 is such an estimated line for Case 2 obtained by correcting the Weibull distribution of Case 1. As shown in Fig. 14a, the estimated Weibull distribution of Case 2 agrees well with the results of thermal stress tests for Case 2. The same procedure was applied to Case 3, and the estimated line for Case 3 is shown in Fig. 14b. As for Case 3, experimental data are separated into two categories. One agrees well with the estimated line, and another exceeds the estimated line. That is, the estimated line gives conservative failure stresses for Case 3.

Next the results of the thermal stress tests are compared with those of the four-point bending tests. The estimated line for the thermal stress tests were obtained from the four-point bending tests by correcting a size effect, using a return period T defined by $T = S/s$, where S and s are effective areas for the thermals stress tests and the four-point bending tests, respectively. As mentioned before, S is an area of the rim surface of a cylindrical slab for the thermal stress tests. On the other hand, s is selected as an area of the outer surface between two supports of the four-point bending test, on which the maximum tensile stress is acting. Such an estimated line is depicted in Fig. 15 as the estimated line 1, together with the Weibull plots of each case of the thermal stress tests and the four-point bending tests.

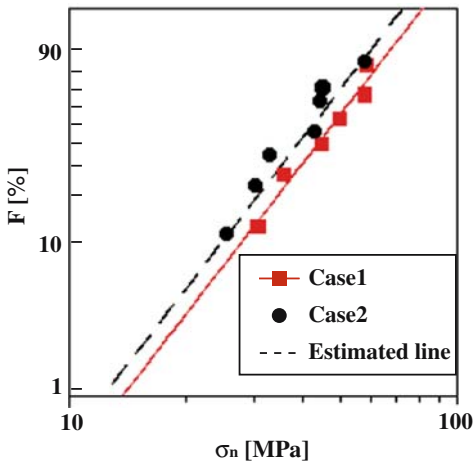

(a) Case 2

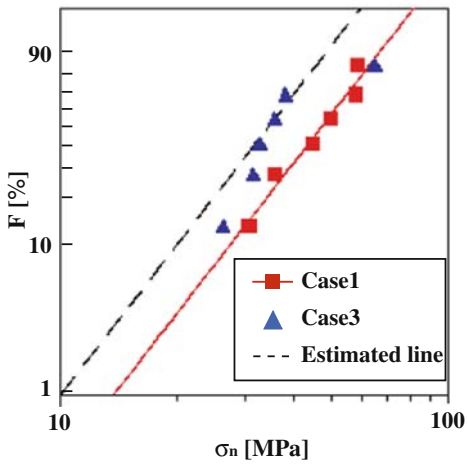

(b) Case 3

Fig. 14 Comparison between Weibull distribution estimated from Case 1 with experimental data. (**a**) Case 2. (**b**) Case 3

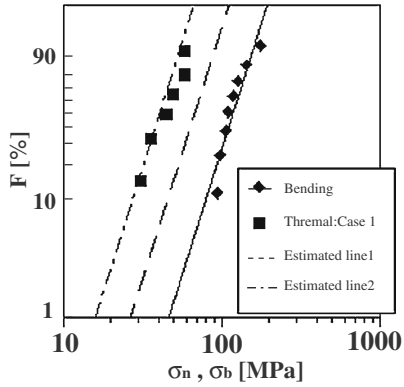

(a) Case 1

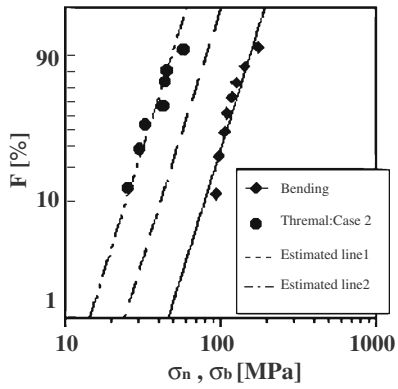

(b) Case 2

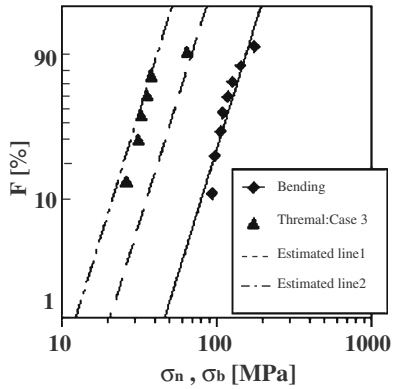

(c) Case 3

Fig. 15 Comparison between Weibull distribution estimated from four-point bending tests with experimental data. (**a**) Case 1. (**b**) Case 2. (**c**) Case 3

Although the estimated line 1 overestimates the failure stress of the thermal stress tests for every case of the thermal stress tests, the difference seems to be nearly the same degree for every case. So the estimated line 2 was obtained from multiplying the estimated line 1 by 0.6. As shown in Fig. 15, the estimated line 2 agrees well with the Weibull plots of the thermal stress tests for every case. Although there is no physical meaning in the factor of 0.6, it is very useful for industrial applications, because the cracking due to thermal stress can be predicted from the four-point bending strength, which can be obtained from a simple test.

Concluding remarks

The thermal stress of an LT single crystal test slab at the time of cracking was calculated using the surface temperatures measured in the thermal stress test. The size effect on the stress for the cracking was investigated using different sizes of test slabs in the thermal stress tests. The four-point bending tests were also performed to examine the relationship between the cracking due to thermal stress and the failure due to mechanical loading. The Weibull plots of failure stress were used for these discussions.

It is found from the results of thermal stress analyses and the observation of the cracking in the test slabs that the cracking induced by thermal stress occurs mainly in the cleavage planes due to the stress component normal to the plane. As for a size effect of failure stress in the thermal stress tests, large-sized test slabs show lower failure stress than small-sized ones. A useful relation was derived for predicting the failure stress due to thermal stress from the four-point bending strength.

Acknowledgements The authors would like to express their gratitude to Koike Co. Ltd. for supplying lithium tantalate test specimens. This study was financially supported by a Grant-in-Aid for Scientific Research from the Japan Society for Promotion of Science.

References

1. Brandle CD, Miller DC (1974) J Cryst Growth 24/25:432
2. Brice JC (1977) J Cryst Growth 42:427
3. Lee SH, Kim YJ, Cho SH, Yoon EP (1992) J Cryst Growth 125:175
4. Galazka Z (1999) Cryst Res Technol 34:635
5. Miyazaki N, Uchida H, Tsukada T, Munakata T (1996) J Cryst Growth 162:83
6. Kobayashi M, Tsukada T, Hozawa M (2002) J Cryst Growth 241:241
7. Miyazaki N, Hattori A, Uchida H (1997) J Mater Sci: Mater Electron 8:133
8. Miyazaki N, Tamura T, Yamamoto K (2000) Comput Model Eng Sci 1:99
9. Smith RT, Welsh FS (1971) J Appl Phys 42:2219
10. Lin TH, Edwards D, Reedy RE, Das K, Mcginnis W, Lee SH (1988) Ferroelectrics 77:153
11. Miyazaki N (2002) J Cryst Growth 236:455
12. Nye JF (1957) Physical properties of crystals. Clarendon Press, Oxford, p 131
13. Choy MM, Cook WR, Hearmon RFS, Jaffe H, Jerphagnon J, Kurtz SK, Liu ST, Nelson DE (1979) LANDOLT-BORNSTEIN numerical data and functional relationships in science and technology, New Series, vol 11. Springer-Verlag, p 53
14. Bansal GK, Duckworth WH, Niesz DE (1976) J Am Ceram Soc 59:477
15. Tsuge H (1987) J Soc Mater Sci Jpn 36:35